Journal of
Composites Science

MDPI

Article

Mechanical and Tribological Behavior of LM26/SiC/Ni-Gr Hybrid Composites

Suyash Y. Pawar [1,*], Julfikar Haider [2,*], Giuseppe Pintaude [3], Santhosh Mozhuguan Sekar [4], Vikram Kolhe [5], Kailas Chandratre [6], Sandipkumar Sonawane [1] and Parmeshwar Ritapure [7]

1 Department of Mechanical Engineering, MVPS's KBT College of Engineering, Nashik 422013, India; sonawane.sandipkumar@kbtcoe.org
2 Department of Engineering, Manchester Metropolitan University, Manchester M1 5GD, UK
3 Academic Department of Mechanics, Universidade Tecnológica Federal do Paraná, Curitiba 81280340, PR, Brazil; pintaude@utfpr.edu.br
4 Faculty of Engineering, Technology and Built Environment, UCSI University, Kuala Lumpur 56000, Malaysia; mozhuguan.santhosh@gmail.com
5 Department of Mechanical Engineering, Late G.N.Sapkal College of Engineering, Nashik 422213, India; kolhe.vikram@gmail.com
6 Department of Mechanical Engineering, KVN NSPS's LGM Institute of Engineering Education and Research, Nashik 422005, India; ckailas@rediffmail.com
7 Department of Mechanical Engineering, Zeal College of Engineering and Research, Pune 411041, India; ritapurep@yahoo.co.in
* Correspondence: suyashyp@gmail.com (S.Y.P.); j.haider@mmu.ac.uk (J.H.)

Abstract: The study evaluates the mechanical and wear properties of LM26 alloy and its hybrid composites with silicon carbide (SiC) and nickel-coated graphite (Ni-Gr). LM26 aluminum alloy is generally known for its high strength, wear, and corrosion resistance compared to similar materials such as zinc and magnesium. The effect of Ni-Gr was studied, with 2 wt.% was found to provide the best mechanical properties. LM26 composites reinforced with varying percentages of SiC (0 to 30 wt.%) showed the best properties at 20 wt.% reinforcement after fabrication using a bottom pouring type stir casting setup (Two step feeding method). Evaluation of five hybrid LM26 composites through tensile strength, elongation, hardness, impact, porosity, and thermal studies showed that the LM26/2 wt.% Ni-Gr/20 wt.% SiC configuration showed the best filler composition for improved strength. Sliding wear evaluation using experimental and Taguchi analysis was performed at different configurations to identify the best wear resistance. Microstructure studies showed the presence of Ni-Gr particles forming coatings and temperature playing a significant role in the progression of the wear rate. Furthermore, the hybrid composite with 20% SiC and 2% Ni-Gr reinforcement showed the best wear resistance.

Keywords: LM26 alloy; hybrid composites; mechanical properties; wear properties; stir casting; Taguchi analysis; microstructure

Citation: Pawar, S.Y.; Haider, J.; Pintaude, G.; Sekar, S.M.; Kolhe, V.; Chandratre, K.; Sonawane, S.; Ritapure, P. Mechanical and Tribological Behavior of LM26/SiC/Ni-Gr Hybrid Composites. *J. Compos. Sci.* **2023**, *7*, 159. https://doi.org/10.3390/jcs7040159

Academic Editor: Francesco Tornabene

Received: 9 March 2023
Revised: 31 March 2023
Accepted: 9 April 2023
Published: 12 April 2023

1. Introduction

Composite materials, known as metal matrix composites (MMCs), are created by combining a matrix material, such as aluminum, titanium, magnesium, or copper, with reinforcement materials, such as carbides, metallic oxides, borides, nitrides, or non-metallic materials such as red mud or fly ash [1–4]. The reinforcement materials are dispersed throughout the matrix and provide improved properties over the matrix alone, and slower degradation than the reinforcement materials alone. Reinforcing aluminum with metallic materials is a common practice in industrial applications and has been the subject of much research in recent years to improve stiffness and strength [5]. However, using reinforcement materials such as nitrides, carbides, and borides oxides can present machining challenges

and lead to abrasion, cracking, and premature failure. Choosing the best reinforcement material for an aluminum matrix is an ongoing focus for scientists and engineers [6–8].

MMCs combine metal matrix and reinforcing phases using liquid-state processing routes such as stir casting, powder metallurgy, and spray deposition, and solid-state fabrication routes such as mechanical alloying, friction stir, and sintering [9,10]. The stir-casting route is advantageous due to its simplicity, flexibility, and high production rate. However, it has drawbacks, such as gas entrapment, reinforcement particle fracture, and agglomeration. A well-dispersed reinforcement in the matrix material, wettable characteristics between the matrix and reinforcements, and adequate porosity levels are all essential elements for obtaining optimal properties in MMCs [11–14].

Researchers worldwide demonstrated that nano fillers greatly influence the properties of AMCs (aluminum matrix composites). Jia et al. [15] used nanofillers (NFs) to develop AMCs through the ultrasonic-assisted process and reported better dispersion of fillers into the matrix. Similarly, Choi and Awaji [16] developed a novel AMC containing various proportions of nanoparticle sizes (10^{-9} m) and investigated its properties. The authors asserted that NFs support molecular bonding of matrix and elaborate dispersion reasonably. Nano-sized particles evenly distributed in the matrix show very low dislocations during fabrication. This phenomenon effectively contributes towards strength enhancement and limits pores drastically [17].

Silicon carbide considerably has predominant properties such as high modulus and thermal and electrical performance and economical with similar grade reinforcements. Bhushan et al. [18] reported after conducting experiments on AMCs that SiC inclusion increased mechanical properties by up to 200% and significant improvement in internal molecular arrangements of fillers into the matrix. Silicon carbide particles are also well known for their wear properties. Kumar et al. [19] developed AA7075/SiC composites and reported that SiC greatly enhances wear properties and hardness more than the virgin alloys. It mixes with the matrix very well due to the density variation. Kumar et al. [20] also compared the strengths of micro and nano SiC-reinforced AA7075 composites. They reported that nano-size fillers using composites show better tensile, wear behavior, and uniform dispersion than micro-size particles.

Modi et al. [21] compared the wear behavior of stir-casted zinc aluminum alloys with cast iron. They asserted that ZA shows better wear resistance and reasonable friction heating than the cast iron. Results also exhibit that load and velocity influence these properties significantly. Gencaga and Temel [22] investigated the wear behavior of the Zn/Al40/Cu2/Silicon hybrid configuration. They reported that the proposed hybrid samples exhibit the least coefficient of friction and improved wear resistance than bronze composites. Savaskan and Aydiner [23] investigated the effect of Cu on tribological behavior in zinc–aluminum alloys. They concluded that Cu inclusion improves microhardness by up to 40% more than the unreinforced alloy, whereas tensile and wear resistance was enhanced by up to 5%. Unlu [24] conducted a series of tests to analyze materials such as bronze, brass, white metal, copper, zinc, aluminum, and zinc–aluminum alloys to utilize for journal bearings. It was reported that zinc–aluminum alloys have superior mechanical properties. Khonsari and Lin [25] investigated Al40Zn with Cu-filled alloys for its wear and hardness properties and compared it with bronze alloys. They asserted that Cu inclusion in Al40 significantly impacts hardness and wear resistance. Moreover, it enhances tensile properties by up to 3% more than neat and bronze composites.

Numerous researchers worked on the mechanical and tribology behavior study of the hybrid metal matrix composites. Bekir et al. [26] conducted series of tests to analyze various materials such as bronze, brass, white metal, copper, zinc, aluminum, and zinc aluminum alloys to utilize it for journal bearings. They reported that zinc aluminum alloys are greatly admirable in achieving superior mechanical properties. The Taguchi method helps to determine optimal conditions for multiple outcomes, but it has limitations when it comes to optimizing multiple outputs with numerous factors [27,28]. The use of LM26 alloy as a metallic matrix for composites is a recent development and an area that has

not been extensively explored for high-temperature wear environments. By incorporating SiC as a reinforcing material in varying amounts, it is possible to investigate the effects of reinforcement on the mechanical and tribological properties of the composites. The addition of Ni-Gr as a secondary reinforcement is a novel approach for enhancing the tribological properties of the composites.

The current study evaluates mechanical and wear behavior of single (LM26/SiC) and hybrid LM26 composites prepared through stir-casting method. Advanced optimization techniques, such as the Taguchi approach, were employed to achieve optimal composite material suitable for high-temperature applications. The microstructures of the composites were evaluated, and the results were verified through the examination of wear resistance with the optimized conditions obtained through the optimization approach. LM26 has almost all the required properties to utilize in the new era of high-temperature applications. No or very few researchers have attempted to study all the mechanical and wear behavior of AMCs combined. Therefore, this research presents a significant novel contribution to the field of composite materials and provides critical knowledge in investigating their wear and mechanical properties for high-temperature applications.

2. Experimental Methods

2.1. Materials

The LM26 aluminum alloy was reinforced with SiC particles (approximate size: 49 µm) and nickel-coated graphite (approximate size: 24 µm) to improve its composite strength. The nickel coating significantly improves the mechanical properties of graphite, making it more durable, wear-resistant, and robust under high load conditions. Additionally, the nickel coating enhances the adhesion and compatibility between graphite and the underlying substrate, preventing delamination and improving overall performance [29,30]. The composition of the LM26 alloy is detailed in Table 1.

Table 1. Chemical composition of aluminum LM26 alloy.

Elements	Cu	Si	Fe	Mg	Mn	Zn	Ti	Ni	Other	Bal.
wt.%	2.3–4.7	8.4–10.6	1.3	0.6–1.4	0.2	1	0.2	1	0.3	Al.

2.2. Fabrication of Composites

The stir casting method, which includes subsystems such as a magnetic stirrer unit, temperature limiting unit, and mold setups, was employed for the composite fabrication. The fillers were preheated to a temperature of 400 °C to enhance their wettability with the matrix material and to eliminate moisture content. First, SiC particles were added to the molten alloy and then the Ni-Gr particles were added. A crucial aspect of the stir casting process that must be considered during fabrication is the formation of an aluminum oxide layer on the surface of the molten metal, as the aluminum core inside the crucible reacts with atmospheric oxide. This aluminum oxide layer protects the metal and prevents further reaction with the atmosphere. Once the matrix reached its maximum temperature of 700 °C, the preheated fillers were added to the molten metal. The stirrer unit was activated, and the ceramic and molten metal mixture was agitated at 500 rpm for 5–8 min using three-pin impeller blades to mix the matrix and filler thoroughly. Care was taken to ensure that the metal was thoroughly agitated during the mixing process and that the vortex entirely absorbed the filled ceramic particles. After mixing, any excess slurry on the metal surface was removed using a scraper, and the molten metal was poured directly into a preheated mold (at 100 °C) after removing the slag floating on the molten metal surface. The composite material was allowed to cool to room temperature for ten hours before being removed from the die.

Abrasive cutters and automatic CNC lathe machines were used to prepare specimens. The abrasive processed metal cast samples were thoroughly prepared for testing, including mounting, polishing, and gold coating. Single LM26/SiC composite samples were prepared

by varying SiC (5, 10, 15, 20, and 30 wt.%). The optimum Ni-coated graphite amount was determined by adding different percentages of 1.0, 2.0, and 3.0 wt.% in LM26 alloy. Finally, hybrid LM26/SiC/Ni-Gr composites were prepared with the optimum amount of Ni-Gr and varying SiC amounts. Various filler compositions were selected for the fabrication of MMCs, and the composite configurations and their constitutions are listed in Table 2 with their respective sample codes. Neat LM26 was also prepared as a reference material for comparison with other composites.

Table 2. Hybrid configurations of AMCs.

Designation	Sample Code	Composition (Weight Percentage)
Matrix alloy	NEAT Sample	Aluminum LM26
Hybrid Composition	HAMC1	Aluminum LM26 + Ni-Gr (02 wt.%) + SiC (05 wt.%)
	HAMC2	Aluminum LM26 + Ni-Gr (02 wt.%) + SiC (10 wt.%)
	HAMC3	Aluminum LM26 + Ni-Gr (02 wt.%) + SiC (15 wt.%)
	HAMC4	Aluminum LM26 + Ni-Gr (02 wt.%) + SiC (20 wt.%)
	HAMC5	Aluminum LM26 + Ni-Gr (02 wt.%) + SiC (30 wt.%)

2.3. Composite Characterization

2.3.1. Tensile Test

Tensile tests of the hybrid samples were carried out using a computerized Unitech—Instron 4001 series ISO 7500-1 standard UTM machine equipped with HIGH TOWN LBG, Italy. Initially, the specimens were prepared as per ASTM E8/E8M standard (12.5 mm diameter × 50 mm gauge length) for the testing with a loading rate of 1 mm/ min. The surfaces of the samples were polished using emery sheets (900 grit) to remove debris and dust. The core objective of the testing is to identify the difference in yield, elongation, and ultimate strengths of the materials. For each configuration, three samples were prepared, and average results were reported.

2.3.2. Impact Test

A Charpy V notch impact test was performed to evaluate the maximum energy absorption capacity of the prepared samples. Tests were conducted using a ball-type pendulum impact tester of ISO 1757: 1988 standard with the sample dimensions of 55 mm × 10 mm × 10 mm (V notch angle of 45 degrees).

2.3.3. Hardness Test

B 3000 model Brinell hardness tester was utilized to evaluate the samples' hardness. Indentations were performed at different locations of samples, and average results correspond to a series of 5 measurements.

2.3.4. Porosity/Void Measurement

It was essential to measure the density and porosity level of the material to use it for diversified weight-cantered applications. The theoretical and experimental densities were calculated separately and compared for obtaining accurate results. The amount of porosity of the fabricated samples was calculated using the following equations.

$$\text{Porosity\%} = (\text{Theoretical Density} - \text{Experimental density})/(\text{Theoretical Density}) \times 100 \quad (1)$$

$$\text{Theoretical Density of composite } (\rho_c) = (\rho_m \times V_m) + (\rho_r \times V_r) \quad (2)$$

where ρ_m and ρ_r are the density of the matrix and reinforcement, respectively. V_m and V_r are the volume fraction of the matrix and reinforcement, respectively.

$$\text{Experimental density} = (W_{air})/((W_{air}) - (W_{medium})) \times \text{Density of medium} \quad (3)$$

where, Density of medium = Density of Ethanol = 0.791 (g/cm^3), W_{air} = Specimen Weight in the air (g), and W_{medium} = Specimen weight in ethanol (g).

2.3.5. Sliding Wear Test

A pin-on-disc tribometer with a standard disc and rig arrangement was utilized for sliding wear tests. EN-24 (shaft steel) with surface roughness (Ra) of 0.3 µm and hardness of 50 HRC was used as a tribopair.

In this research, EN 24 shaft was effectively used against the proposed hybrid aluminum composites for advanced wear performance study. Pin diameter ranges from Φ3 mm to 12 mm, pin temperature is about Min: ambient to Max: 400 °C, load and disc rotation speed varies from 5 N to 200 N and 200–2000 RPM respectively. At the same time, the various wear process parameters such as sliding distance (50–400 m), speed (100–600 rpm), applied load (10–60 N), and temperatures (50–250 °C) are varied while testing the wear resistance of the samples.

2.3.6. Microscopical Observation

The microscopic image of the unfractured and fractured samples was captured using an FEI Quanta 400F Field Emission microscope with an accelerating voltage of 10 kV. Similarly, samples are mirrored polished and thoroughly polished using emery sheets, then mounted in the mold for examination.

3. Results and Discussions

3.1. Selection of Matrix Alloy and Ni-Gr Content

LM26 is an aluminum-based alloy from the aluminum-silicon-magnesium alloy family. It is a high-strength alloy that is primarily used for its excellent casting properties, high-temperature strength, and corrosion resistance. LM26 is a highly adaptable alloy that finds widespread use across several industries such as aerospace, marine, automotive, and industrial applications. In the proposed research, the LM26 alloy was examined and compared to similar materials such as zinc, magnesium, and pure aluminum. Analysis was performed, and results were documented, including elongation, impact energy absorption, hardness, and tensile strength measurements for various materials, as shown in Figure 1. The microstructure and elemental analysis of the matrix material are depicted in Figure 2. The results indicated that the LM26 alloy had better wettability between all types of ceramics reinforced within it [3]. By optimizing the distribution and dispersion of ceramic particles in the matrix, the mechanical properties of the composite are improved. The LM26 alloy, an aluminum-based alloy, contains copper, magnesium, and manganese, in addition to aluminum. Copper enhances the alloy's strength and hardness, while magnesium improves its ductility and toughness. Furthermore, the addition of magnesium enhances the alloy's ductility, allowing it to deform without fracturing. The mechanical properties are also enhanced by the refined grain structure, which lowers the probability of flaws and improves the material's strength and toughness. Manganese is also beneficial in refining the alloy's grain structure, improving its mechanical properties. The LM26 alloy exhibited the highest elongation, impact energy absorption, and reasonable hardness improvement. Based on these findings, the LM26 alloy was preferred for its superior properties as a matrix material. EDS analysis confirmed the elemental composition of the LM26 alloy. The mechanical behavior of the LM26 alloy looks excellent when compared to the other materials [9,14,23].

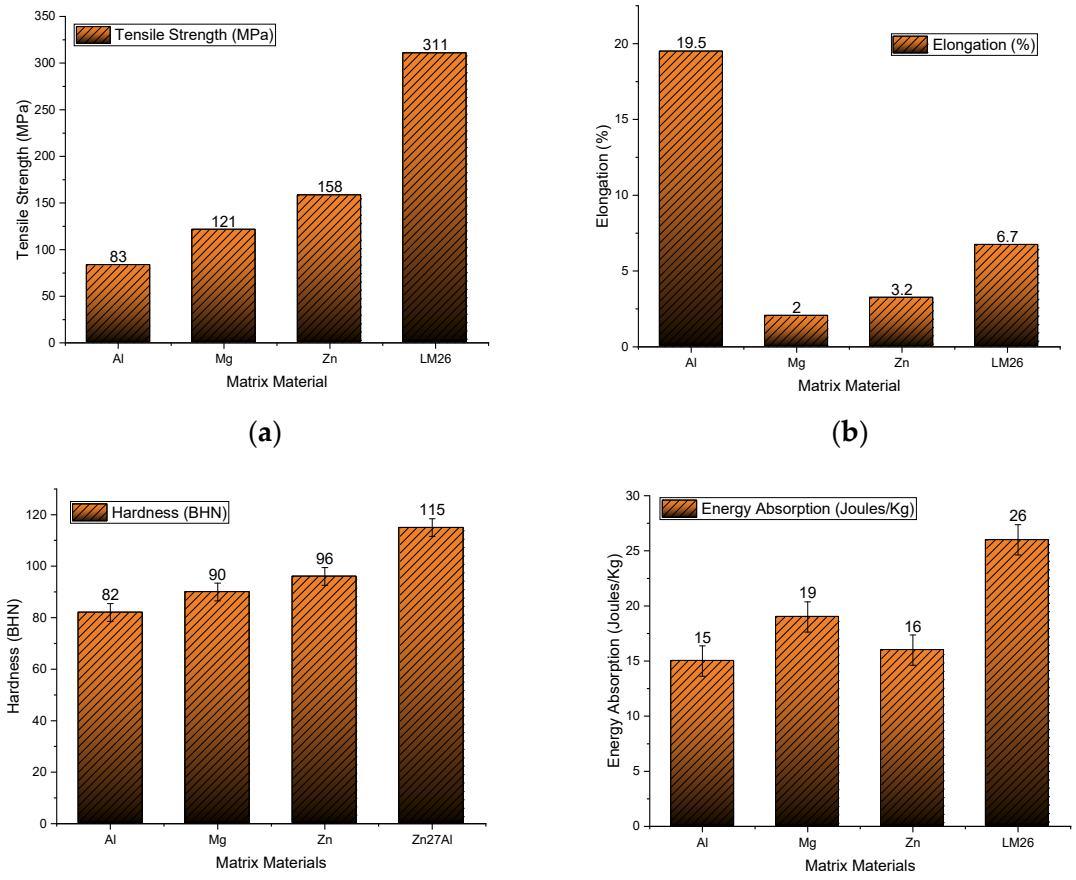

Figure 1. (**a**) Tensile strength, (**b**) Elongation, (**c**) Hardness, (**d**) Impact energy absorption results of different matrix materials.

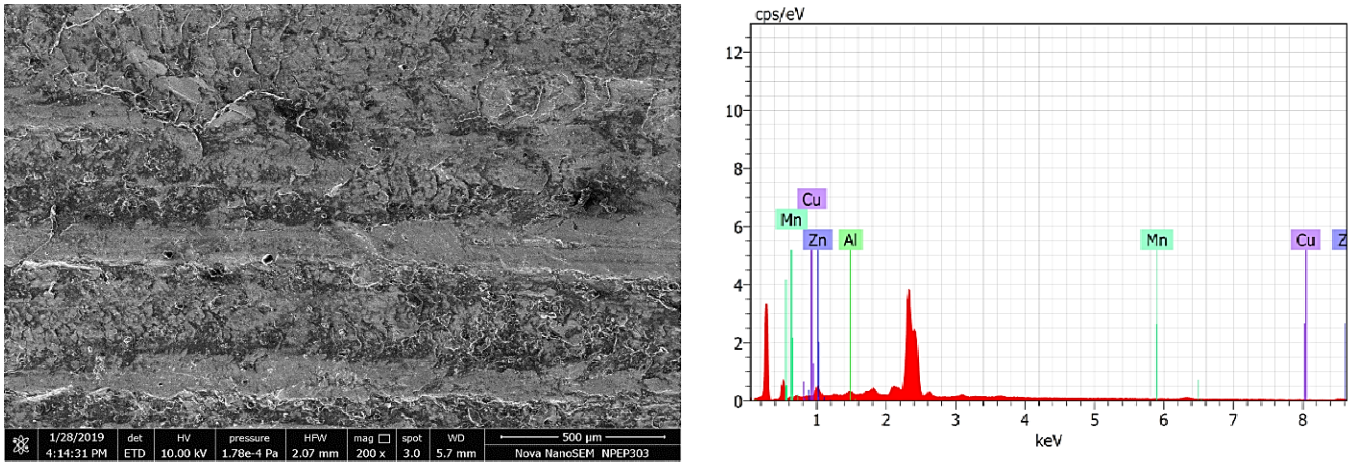

Figure 2. (**a**) SEM Micrograph and (**b**) EDS map of LM26 Al alloy.

Although graphite improves wear resistance through its inherent solid lubrication effect, but its load bearing capacity is still poor. By coating Ni on the graphite can improve its mechanical properties and resists the agglomeration of graphite in the LM26 alloy matrix [31,32].

3.2. Mechanical Characterization of LM26/Ni-Gr Composites

The physical and mechanical properties of LM26 alloy filled with various weight percentages of nickel-coated graphite (Ni-Gr) were investigated to find the optimum amount of Ni-Gr filler for the best mechanical and tribological properties. Initial experiments were conducted with 1, 2, and 3 wt.% Ni-Gr-filled composites and compared to LM26 alloy or unfilled composites. The difference between theoretical and experimental densities, and the porosity levels, was reported along with mechanical characterization. Figure 3 illustrates the observed results from the experiments. Theoretical and experimental densities revealed that porosity gradually increased with the filler percentages. Microscopic images of LM26/Ni-Gr composites revealed the presence of small pores and voids on the surface of the samples (Figure 4).

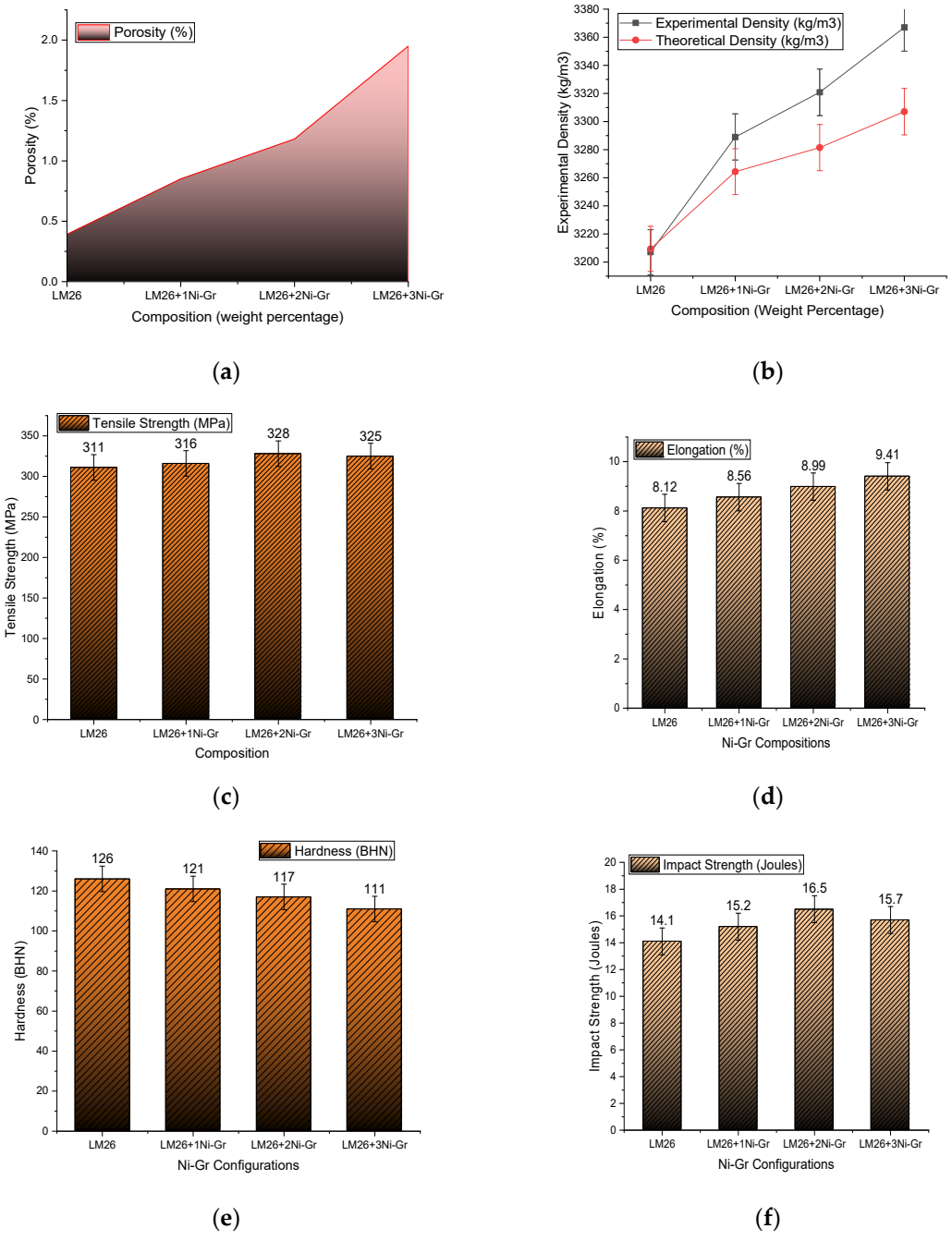

Figure 3. (**a**) Porosity level, (**b**) Experimental and theoretical density comparison, (**c**) Tensile strength, (**d**) Elongation, (**e**) Hardness, and (**f**) Energy absorption capacity of LM26 + Ni-Gr Composites.

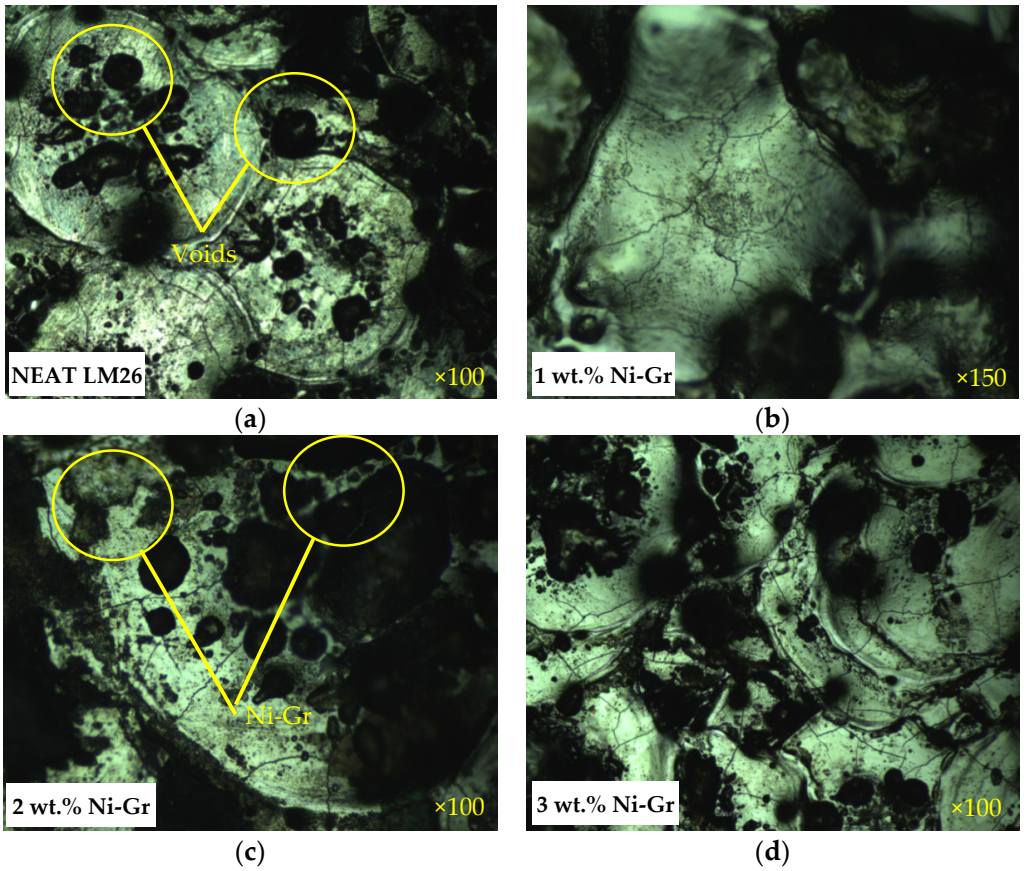

Figure 4. Metallurgical microscopic images. (**a**) Neat LM26, (**b**) 1 wt.% Ni-Gr, (**c**) 2 wt.% Ni-Gr, (**d**) 3 wt.% Ni-Gr.

Tensile strength increased with the filler percentages up to 2.0 wt.%, but slightly decreased with a further increase in the Ni-Gr amount [33]. A similar trend was also noticed for the impact strength. On the other hand, Brinell hardness values gradually reduced due to the softness of the graphite particles [34]. Both density and ductility or elongation percentages increased with the increasing concentration of Ni-Gr, again for the same reason of softer graphite particle introduction. Mendoza [35] reported that Ni-Gr addition in the aluminum matrix possess lower porosity and improved mechanical performance along with the significant wear resistance. Therefore, it was concluded that 2.0 wt.%, Ni-Gr reinforced particles could provide a better combination of strength, hardness, density, and ductility.

3.3. Mechanical and Microstructural Characterization of SiC/LM26 Composites

As shown in the LM26 + Ni-Gr single composite, the hardness decreased due to the addition of softer graphite, a hybrid composite with the introduction of harder SiC has been proposed. Tensile strength, hardness, and energy absorption properties of the LM26/SiC composites gradually increased up to 20 wt.% of SiC reinforcements and decreased after that (Figure 5). The ductility of the composites drastically reduced with the SiC reinforcement, while the porosity was found to increase. The results indicated that up to 20 wt.% SiC reinforcement resulted in superior properties, and this configuration is proposed for further examination. The morphology of 30 wt.% SiC reinforced composites at different magnifications were captured using an Olympus microscope and presented for discussion in Figure 6. It was evident that pores and small voids were present in the contour, and clusters of SiC were also found in the samples, which may contribute to a reduction in strength [36,37].

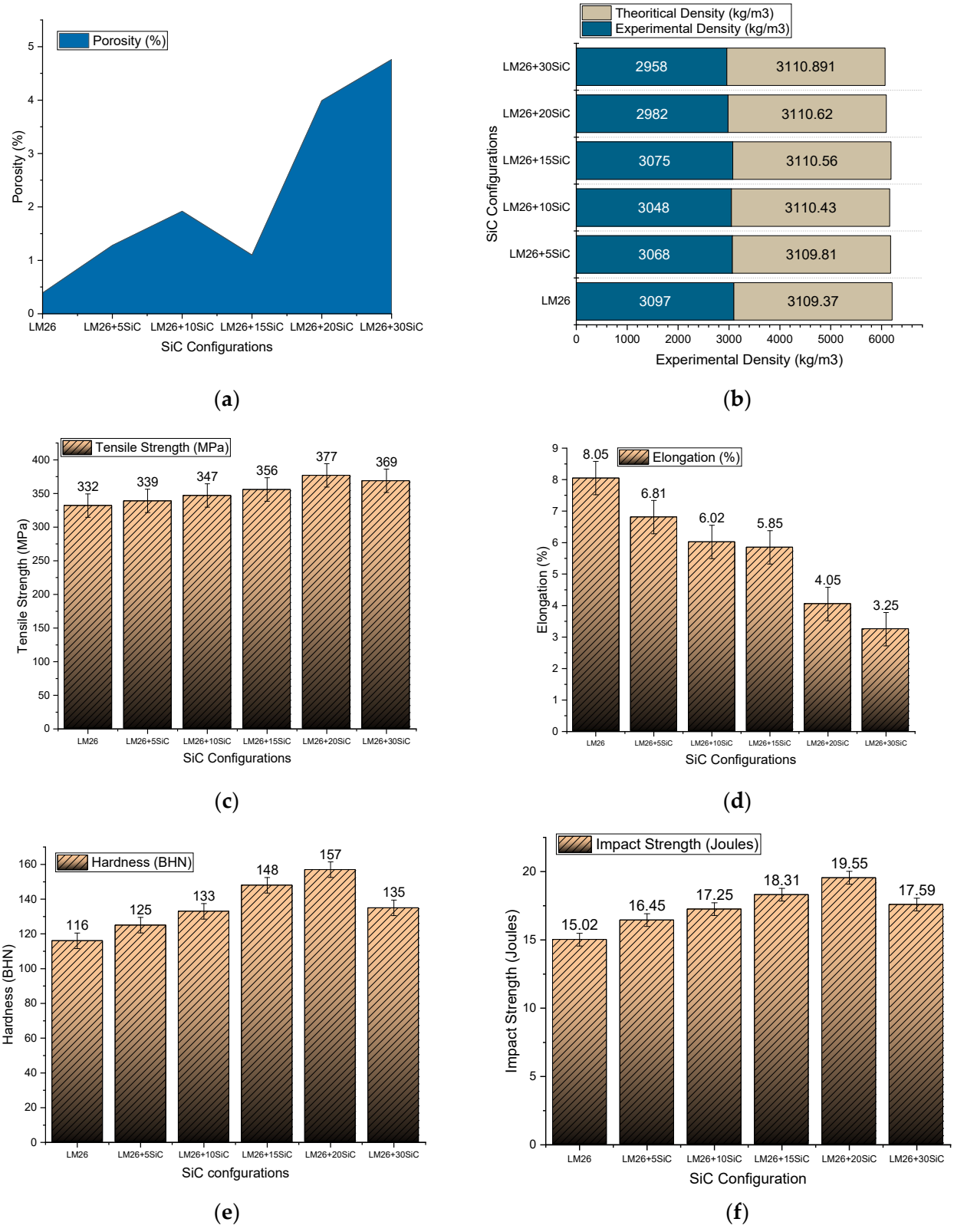

Figure 5. (**a**) Porosity level, (**b**) Experimental and theoretical density comparison, (**c**) Tensile strength, (**d**) Elongation, (**e**) Hardness, and (**f**) Energy absorption capacity of LM26/SiC Composites.

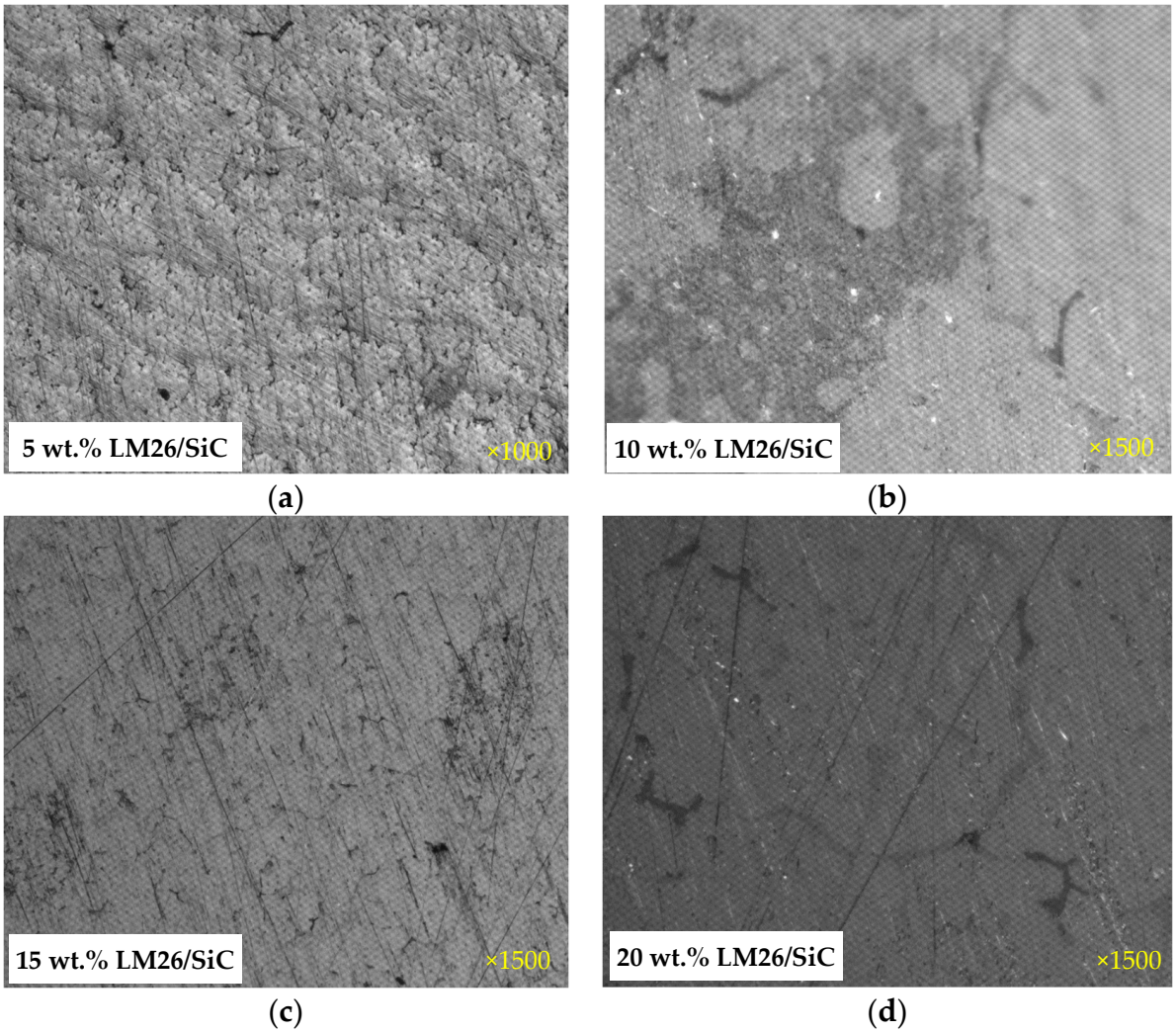

Figure 6. Metallurgical microscopic images of LM26/SiC composites at different magnifications (**a**) 5 wt.%, (**b**) 10 wt.%, (**c**) 15 wt.%, (**d**) 20 wt.%.

3.4. Mechanical Characterization of Hybrid Aluminum Composites

Tensile, elongation, hardness, impact, and porosity values of the hybrid LM26/SiC/Ni-Gr composites are presented in Figure 7. The results of the tensile studies indicate that the HAMC4 configuration exhibited superior elongation and strength compared to other compositions. Hardness also increased gradually with increasing filler percentages but reached a limit with further additions of SiC particles [38]. In summary, the general trend in single and hybrid composites was similar. However, higher ductility and impact energy (except HAMC5) were found in the hybrid composites compared to the single composites and neat alloys. On the other hand, the hybrid composites at the optimum concentration of SiC (20 wt.%) showed lower strength and hardness than their single counterparts.

The microstructure of the hybrid samples was thoroughly examined using a microscope at magnifications ranging from ×150–200, and the results are presented in Figure 8. It is evident from the images that there is a smooth distribution of micro-constituents on the matrix. The characterization studies revealed that the HAMC4 composite is reinforced with 20 wt.% SiC and 2 wt.% Ni-Gr exhibits superior results. SEM and EDS analyses were performed on the HAMC4 composite to validate the study further and the results are presented in Figure 9.

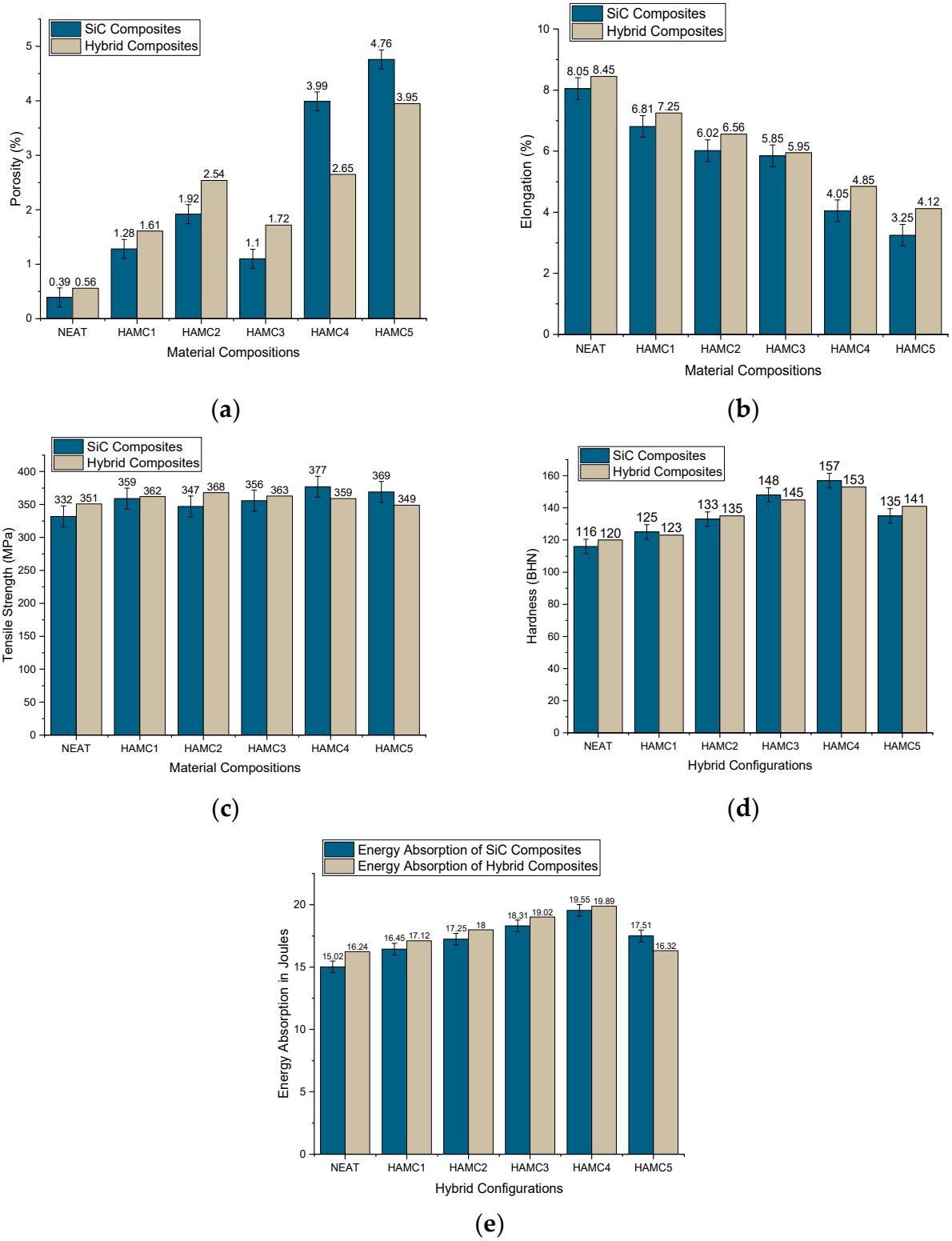

Figure 7. (**a**) Porosity level, (**b**) Elongation, (**c**) Tensile strength, (**d**) Hardness, and (**e**) Energy absorption capacity of hybrid composites.

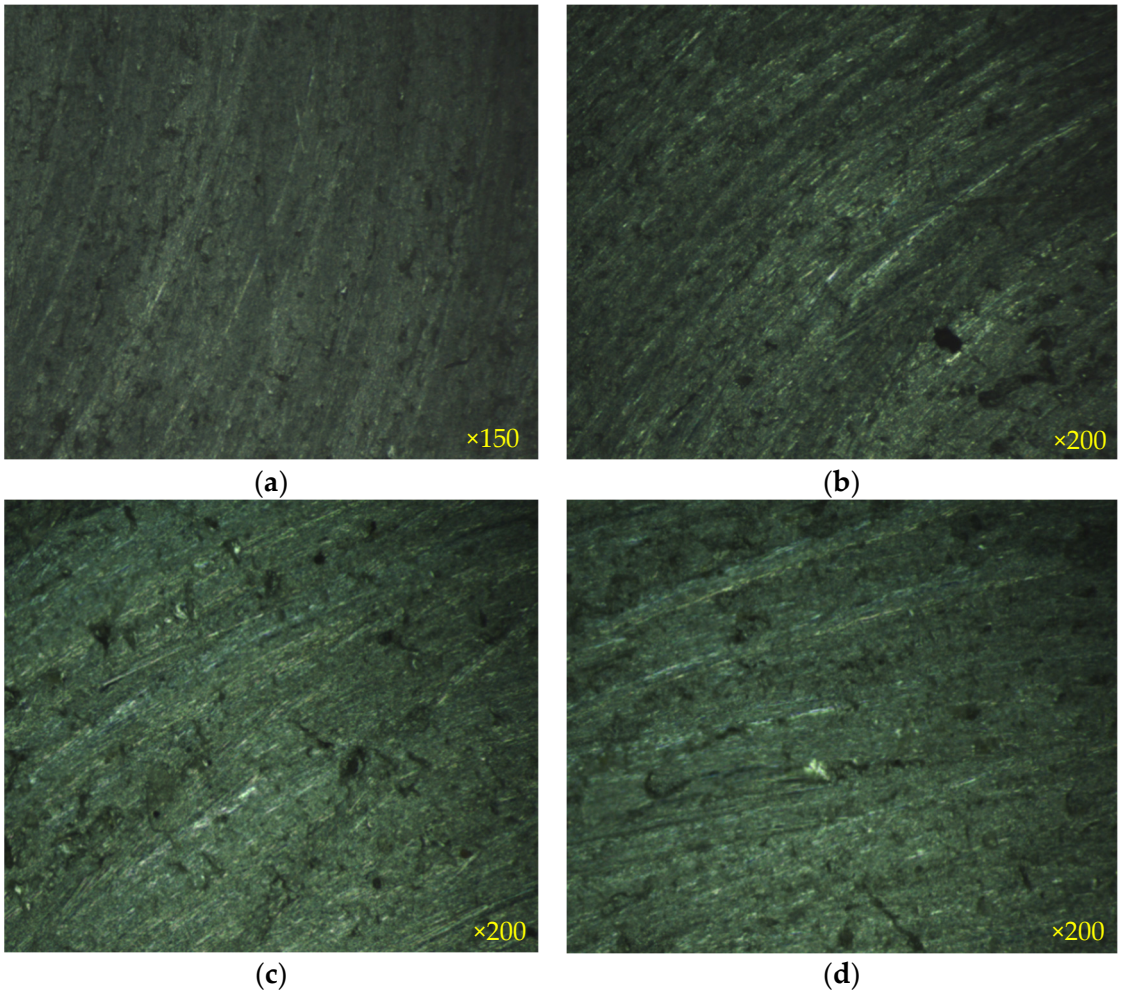

Figure 8. Metallurgical microscopic images of hybrid composites at different magnifications from ×150–200: (**a**) neat sample hybrid composites with 2 wt.% Ni-Gr and (**b**) 5 wt.% SiC, (**c**) 10 wt.% SiC, and (**d**) 20 wt.% SiC.

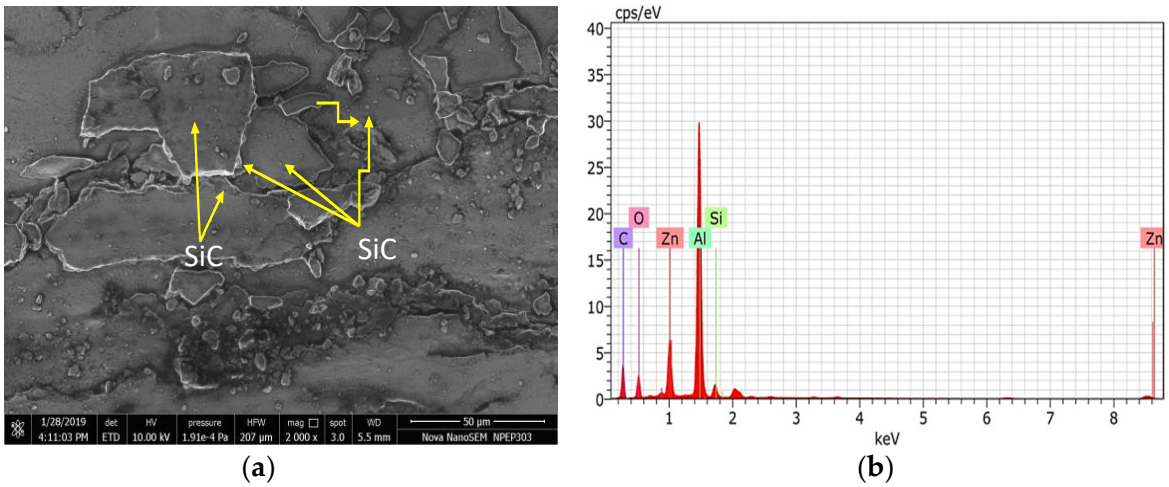

Figure 9. (**a**) SEM micrograph and (**b**) EDS map of the hybrid samples.

3.5. Hybrid Composites Wear Behavior Analysis

The combination of 2 wt.% Ni-Gr reinforcement and varying weight percentages of SiC (5, 10, 15, and 20%) on the sliding wear behavior of the fabricated hybrid composites were investigated using a standard EN24 disc and various process factors, including temperature,

applied load, filler weight percentage, and sliding velocity, according to L16 orthogonal array. Wear tests were conducted to determine the deviation and accuracy level of the developed models. It was observed from the statistical analysis that the most dominating parameter of wear is temperature, followed by the applied load and filler percentage, and the least dominating parameter was sliding velocity. It was observed that 2 wt.% of Ni-Gr reinforcement exhibits superior wear resistance compared to the other configurations, and 20 wt.% of SiC addition exhibited excellent wear behavior [39].

3.5.1. Taguchi Analysis

After analyzing the process parameters of hybrid configurations using L16 orthogonal array for three samples, its average values were reported in Table 3. A better approach was followed for the optimization, and experimentation was performed using Minitab 18 software. Results in the form of noise-to-signal ratio were reported in Table 4. The difference between each factor's highest and lowest average response values can calculate delta values.

Table 3. Wear results for hybrid configurations as per L16 (4^5).

Test	Sliding Speed (A)	Load (B)	Temperature (°C)	Sliding Distance (D)	Filler Content (E)	Wear (Micron)	SN Ratio
	m/s	N	°C	km	wt.%		
1	1	20	40	1.5	5	186	−45.3903
2	1	40	60	3	10	273	−48.7233
3	1	60	80	4.5	15	349	−50.8565
4	1	80	100	6	20	436	−52.7897
5	2	20	60	1.5	5	281	−48.9741
6	2	40	40	3	10	243	−47.7121
7	2	60	100	4.5	15	401	−52.0629
8	2	80	80	6	20	439	−52.8493
9	3	20	80	1.5	5	350	−50.8814
10	3	40	100	3	10	448	−53.0256
11	3	60	40	4.5	15	313	−49.9109
12	3	80	60	6	20	414	−52.3400
13	4	20	100	1.5	5	407	−52.1919
14	4	40	80	3	10	391	−51.8435
15	4	60	60	4.5	15	430	−52.6694
16	4	80	40	6	20	372	−51.4109

Table 4. Response for SN Ratios.

Level	A	B	C	D	E
1	−49.44	−49.36	−48.61	−50.41	−50.98
2	−50.40	−50.33	−50.68	−50.92	−50.77
3	−51.54	−51.37	−51.61	−51.07	−50.78
4	−52.03	−52.35	−52.52	−51.01	−50.88
Delta	2.59	2.99	3.91	0.66	0.21
Rank	3	2	1	4	5

Figure 10 represents the standard S/N ratio, means of variance, and contour plot with respect to temperature, applied load and wear rate. According to the results, the temperature was found to have the highest rank, followed by the applied load (rank 2), filler weight percentage (rank 4), sliding velocity (rank 3), and sliding distance (rank 5). The delta values also indicated that the higher the delta values, the greater the influence of the parameter. Furthermore, Figure 11 revealed that the optimal wear rates were observed at (A1, with a speed of 1 m/s), (B1, with a load of 20 N), (C1, with a temperature of 40 °C), (D1, with a sliding distance of 1.5 km), and (E2, with a filler content of 20 wt.% SiC). Temperature and wear resistance were inversely proportional, with an increase in one leading to a decrease in the other. However, a filler content of 20 wt.% was observed to result in significantly lower wear rates compared to the other configurations. Results on the response for means are presented in Table 5.

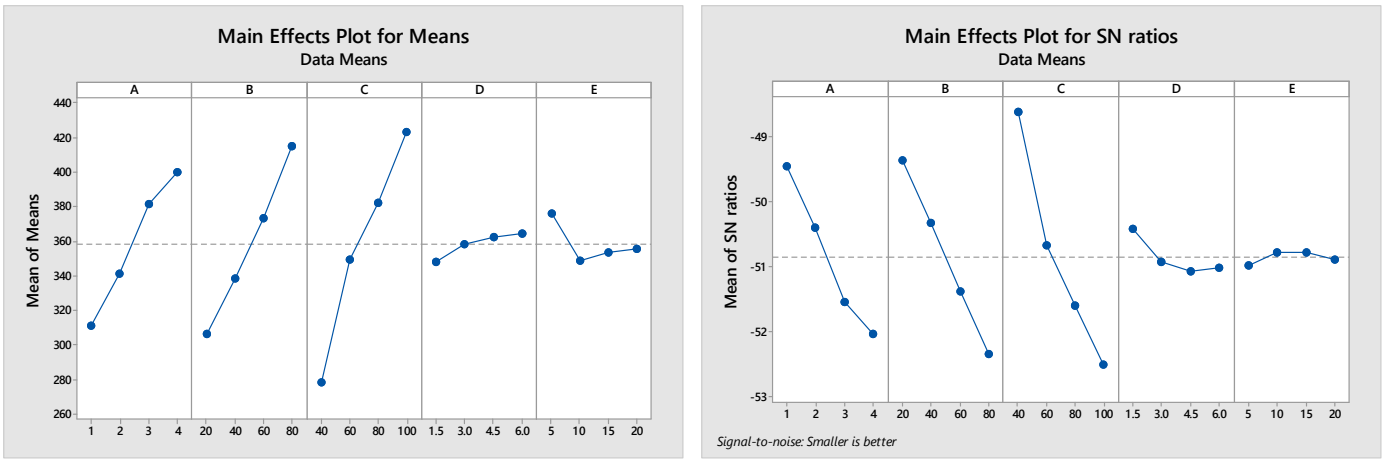

(**a**) (**b**)

Figure 10. Plots for (**a**) Mean and (**b**) S/N ratio.

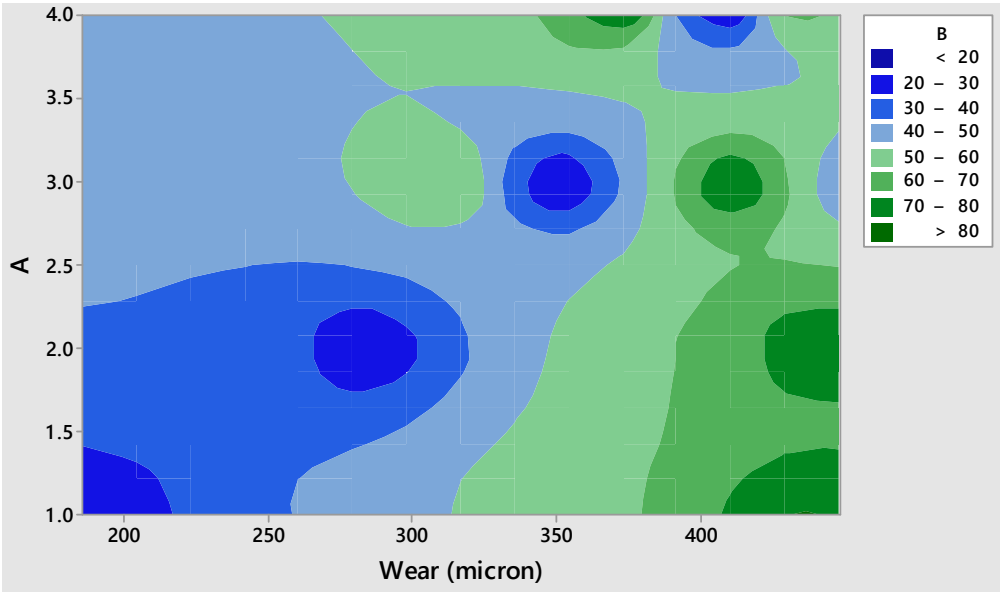

Figure 11. Contour plots for wear vs. sliding speed and applied load.

Table 5. Wear response for average values of each parameter.

Level	A	B	C	D	E
1	311.0	306.0	278.5	348	375.8
2	341.0	338.8	349.5	358	349
3	381.3	373.3	382.3	362.5	353.3
4	400	415.3	423	364.8	355.5
Delta	89	109.3	144.5	16.8	26.8
Rank	3	2	1	5	4

3.5.2. Analysis of Variance (ANOVA)

ANOVA analysis was performed at a confidence level of 95% to calculate the influence of individual parameters on the wear rate. Individual factor significance was calculated using *p*-values and F-values. Less than 0.05% of *p*-values represent the better significance of the parameters. Table 6 describes the *p*-values of all five variables, which are less than 0.05% and significantly contributed to the wear performance of the material. Individual contributions to the specific factors and parameters were also reported. Temperature contributes 36.88%, followed by sliding speed, applied load, sliding distance, and temperature contributing 30.36%, 26.30%, 2.70%, and 1.706%, respectively.

Table 6. ANOVA for wear rate.

Source	DF	SS	MS	F Value	*p*-Value	% Contribution
A	1	18,880.5	18,880.5	65.72	0.000	30.36
B	1	26,245	26,245	91.35	0.000	26.30
C	1	43,477	43,477	151.33	0.000	36.88
D	1	599.5	599.5	2.09	0.16	2.700
E	1	655.5	655.5	2.28	0.159	1.706
Error	10	2823	287.3			2.054

3.5.3. Predictive Equation for Wear Estimation

Input parameters and response relationships were expressed by the regression Equation (4).

$$\text{Wear Rate} = 28.4 + 30.72\ A + 1.811\ B + 2.331\ C + 3.65\ D - 1.145\ E \quad (4)$$

Positive and negative coefficients represent gain and loss in wear rates, respectively. Moreover, the coefficient of determination (R^2) values are close, which means the integration of the derived equation, and undergoes the 95% accuracy level.

3.5.4. Confirmation Experiment

Confirming the experimental optimized results is a stage to authenticate the derived results. Data were analyzed using Minitab optimization represents the optimum parameters of $A_1B_1C_1D_1E_2$, and the results were reported in Table 7. It was also observed that the error rate associated with the experiment is 2.24% which denoted the model has better reliability by up to 95% during the development of the hybrid composites.

Further experiments were conducted to investigate the effect of pin temperature on the wear rate of the proposed composites, as represented in Figure 12. Results depict that increasing temperature gradually accelerates the wear rate due to the internal deformation of the fillers resulting in the failure of the proposed composites.

Table 7. Confirmation Results.

Level	Parameters (Initial)	Parameters (Optimal)		
		Predicted	Experimental	Error
	$A_1B_1C_1D_1E_1$	$A_1B_1C_1D_1E_1$	$A_1B_1C_1D_1E_2$	
Wear	186	178	174	2.24
SN ratio	−44.87	−44.45	−43.95	

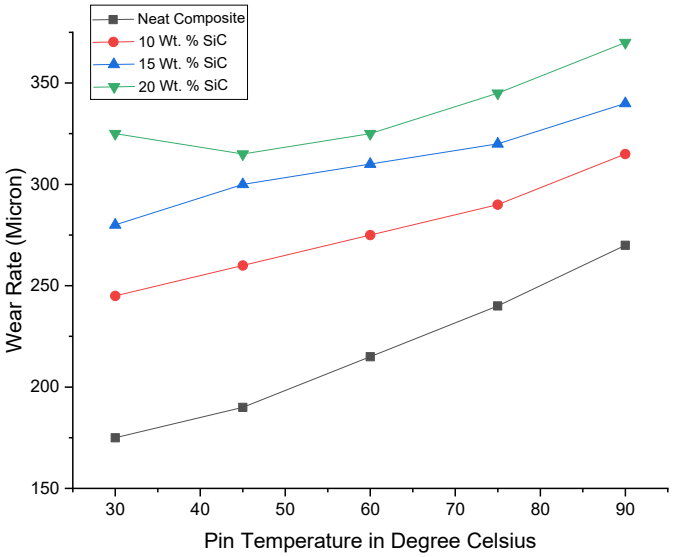

Figure 12. Effect of pin temperature on the wear rate.

3.5.5. Percentage Errors in Experimental and Taguchi Approach

Table 8 illustrates the percentage of wear rate error obtained through both experimental and predicted models. The optimal wear rate for the respective error percentage was analyzed for its reliability calculations. It was observed that the wear rate associated with the wear optimization studies was 2.24%, and it effectively tolerates the wear rates to achieve the highest performance of the proposed samples. The maximum accuracy is contingent upon the error percentage derived from the results and, in this case, the predicted model provides up to 97% accuracy. Additionally, Figures 13 and 14 depict graphical representations of the compared wear rates and respective error percentages.

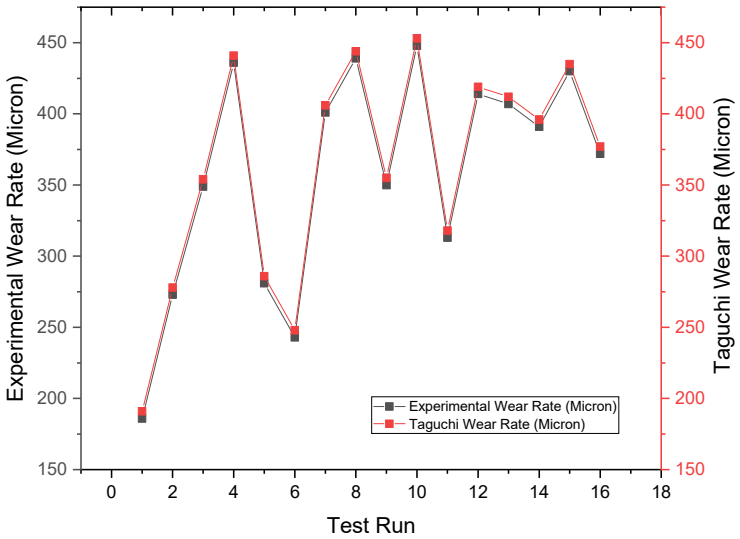

Figure 13. Experimental and Taguchi wear rate comparison.

Table 8. Error percentages in the Taguchi and predicted model.

Test Run	Wear Results (Micron) Experiment and Predicted		Percentage Error in Wear Results	
	Experiment	Taguchi	Experiment	Taguchi
1	186	191	10.2921	3.053878
2	273	278	9.6885	2.494022
3	349	354	10.32361	3.384677
4	436	441	9.91254	−1.24437
5	281	286	5.27093	−2.91348
6	243	248	−0.137161	2.576
7	401	406	−9.93195	0.340658
8	439	444	−1.61118	−1.1356
9	350	355	−9.28481	1.101194
10	448	453	−5.14507	0.97358
11	313	318	−11.7797	−0.89692
12	414	419	−3.86821	−0.58034
13	407	412	8.884387	−0.12203
14	391	396	10.48158	3.177678
15	430	435	3.405672	0.02665
16	372	377	−3.5385	−0.42828

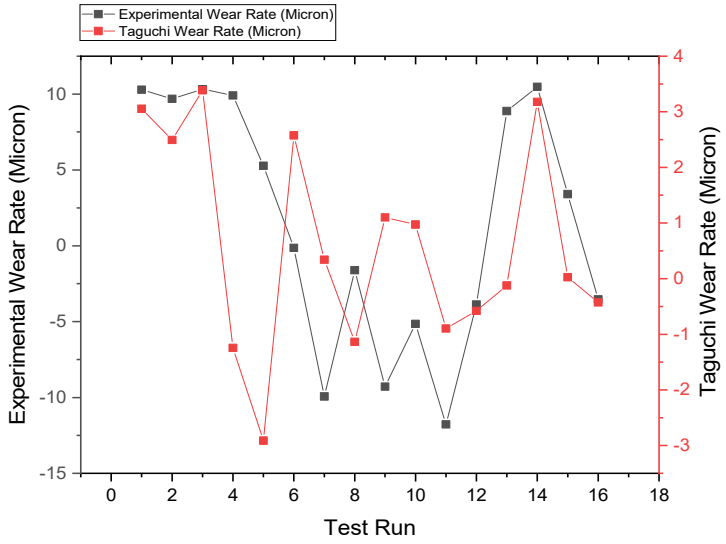

Figure 14. Experimental and Taguchi wear rate error percentage comparison.

3.5.6. Worn Surface Morphology

To understand better the tribological behavior, Figure 15 presents the cross-section of the predicted optimum condition ($A_1B_1C_1D_1E_2$).

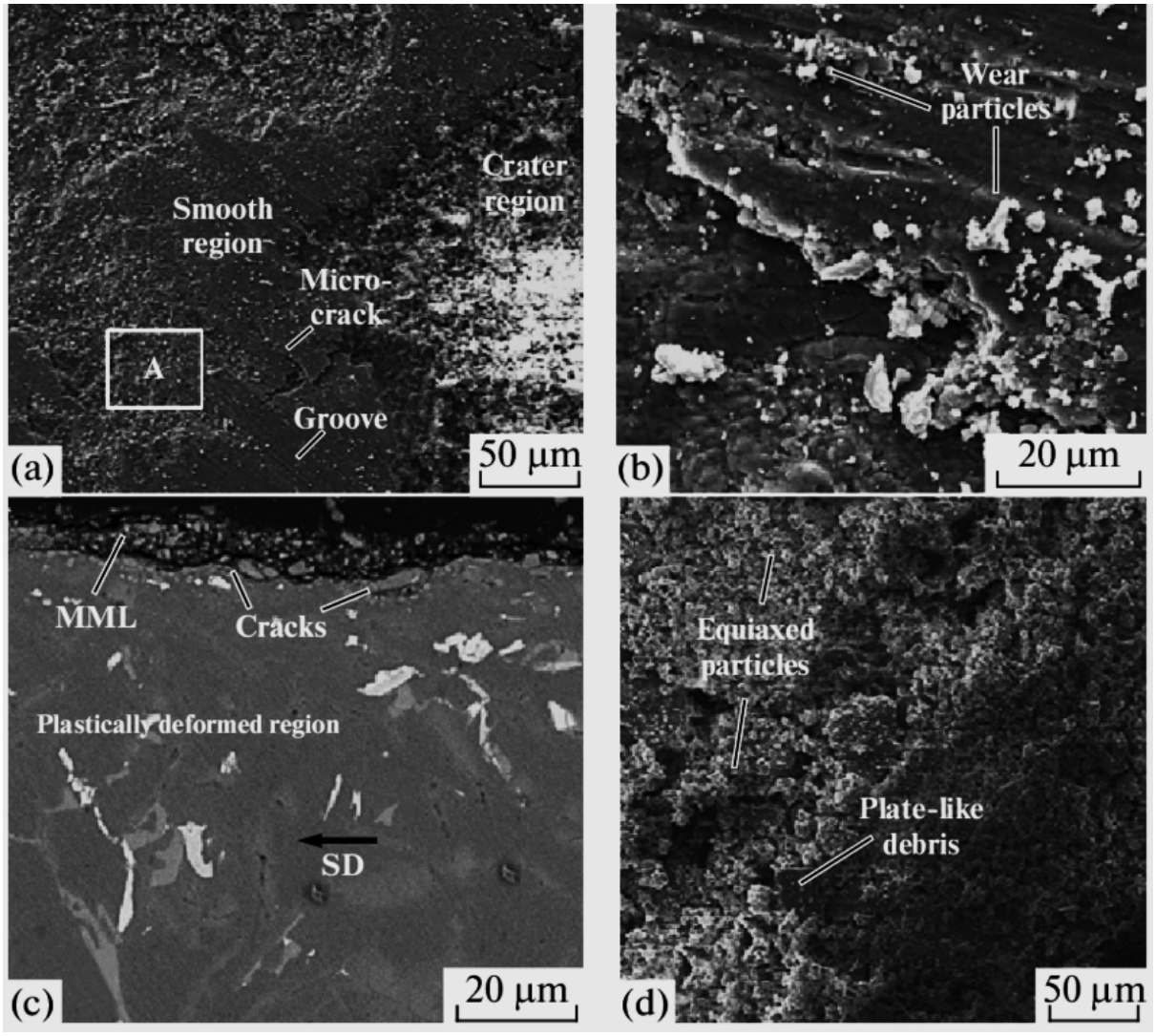

Figure 15. Metallurgical micrographic images of the wear track at the predicted optimum condition (A1B1C1D1E2) for (**a**) Position 1, (**b**) Position 2, (**c**) Position 3, and (**d**) Position 4. SD: Sliding direction and MML: Mechanically mixed layer.

A top layer can be identified at the cross-section, which is a mechanically mixed layer (MML). The formation of this layer is a result of the compression of wear debris, which can be composed by the extrusion of second phases, SiC, and graphite. The continuity of contact stresses led to cracks formation [40].

Figure 15a shows the top surface after the wear process for the same material condition. Figure 15b presents the aspect of the worn surface where micro-cracks formed when the composite is subjected to contact stresses. The eggshell effect can happen, i.e., the level of deformation imposed on the original surface was sufficient to weaken the support given to this top layer [41]. A zoom of the worn surface in Figure 15c reveals the wear debris. The compression of them is a result of the plastic deformation imposed by the contact. This Figure presents many aspects and characteristics of severe plastic deformation. Finally, Figure 15d shows the element of the MML. It is clear its distinctive aspect, confirming the observed in Figure 15a.

4. Conclusions

In order to improve mechanical properties of LM26 alloy compared, five hybrid LM26 composites with SiC contents from 0 to 30% wt.% were prepared. LM26 alloy

composites reinforced with 20 wt.% Silicon Carbide (SiC) was identified to display the best mechanical properties.

To enhance the tribological behavior of composites, Ni-coated graphite (Ni-Gr) was added from 1 wt.% to 3% wt.%, and an optimum content of 2 wt.% was found to maintain the mechanical properties at the high-level.

Using experimental and Taguchi analysis, the composites were tested for wear resistance. A combination between operational variables and filler content resulted in a best wear resistance with accuracy up to 95% was $A_1B_1C_1D_1E_2$ (A_1: 1 m/s, B_1: 20 N, C_1: 40 °C, D_1: 1.5 km, and E_2: 20 wt.% SiC).

Analyzing the worn surfaces, a mechanically mixed layer (MML) was formed, from the extrusion of secondary phases. The imposed deformation was enough to promote cracks along with the MML layer.

Author Contributions: Conceptualization, S.Y.P. and S.S.; methodology, S.Y.P.; validation, S.S., S.Y.P. and J.H.; formal analysis, S.Y.P., J.H., G.P., S.M.S., V.K., K.C., S.S. and P.R.; investigation, S.Y.P. and G.P.; data curation, S.M.S. and V.K.; writing—original draft preparation, S.Y.P., K.C. and S.M.S.; writing—review and editing, V.K., G.P., P.R. and J.H.; visualization, S.M.S. and K.C.; supervision, G.P. and J.H. All authors have read and agreed to the published version of the manuscript.

Funding: This research received no external funding.

Institutional Review Board Statement: Not applicable.

Informed Consent Statement: Not applicable.

Data Availability Statement: The data presented in this study are available within the article.

Conflicts of Interest: The authors declare no conflict of interest.

References

1. Emiru, A.A.; Sinha, D.K.; Kumar, A.; Yadav, A. Fabrication and Characterization of Hybrid Aluminium (Al6061) Metal Matrix Composite Reinforced with SiC, B4C and MoS2 via Stir Casting. *Int. J. Met.* **2022**, 1–12. [CrossRef]
2. Gecu, R.; Karaaslan, A. Sliding Wear of the Ti-Reinforced Al Matrix Bi-metal Composite: A Potential Replacement to Conventional SiC-Reinforced Composites for Automotive Application. *Int. J. Met. Cast.* **2019**, *13*, 641–652. [CrossRef]
3. Asthana, R.; Sobczak, N.; Singh, M. Wettability and interfacial phenomena in the liquid-phase bonding of refractory diboride ceramics: Recent developments. *Int. J. Appl. Ceram. Technol.* **2022**, *19*, 1029–1049. [CrossRef]
4. Khalkho, J.S.; Karunakar, D.B.; Vidyasagar, S. Effect of Aging and Rolling on Microstructure and Mechanical Properties of AA7075/TaC Composites. *J. Mater. Eng. Perform.* **2023**. [CrossRef]
5. Ramadoss, N.; Pazhanivel, K.; Ganeshkumar, A.; Arivanandhan, M. Microstructural, mechanical and corrosion behaviour of B4C/BN-reinforced Al7075 matrix hybrid composites. *Int. J. Met.* **2023**, *17*, 499–514. [CrossRef]
6. Ranjan, S.; Karloopia, J.; Jha, P.K. Recent Advances in Aluminium-Based Hybrid Metal Matrix Composites: A Review. In *Metal-Matrix Composites*; Springer: Cham, Switzerland, 2022; pp. 53–81. [CrossRef]
7. Roy, S.; Albrecht, P.; Weidenmann, K.A. Influence of Ceramic Freeze-Casting Temperature on the Anisotropic Thermal Expansion Behavior of Corresponding Interpenetrating Metal/Ceramic Composites. *J. Mater. Eng. Perform.* **2022**, 1–12. [CrossRef]
8. Gautam, S.K.; Mallik, M.; Roy, H.; Lohar, A.K.; Samanta, S.K. Wear and Mechanical Properties of In Situ A356/5%TiB2 Composite Synthesis by Cooling Slope Technique. *Int. J. Met. Cast.* **2022**. [CrossRef]
9. Pawar, S.Y.; Kharde, Y.R. Tribological characterization of LM26/SiC/Ni-Gr. Hybrid aluminium matrix composites (HAMCs) for high temperature applications. *Mater. Today Proceeding* **2020**, *37*, 793–800. [CrossRef]
10. Pasha, M.B.; Kaleemulla, M. Processing and characterization of aluminum metal matrix composites: An overview. *Rev. Adv. Mater. Sci.* **2018**, *56*, 79–90. [CrossRef]
11. Yilmaz, M.; Kurt, H.I.; Yilmaz, N.F. Correction: Manufacturing and Characterization of Al–xMg–xMgO Composites Using Stir Casting Process. *Int. J. Met.* **2023**, *35*, 105731. [CrossRef]
12. Qiu, M.; Li, Z.; Liu, H.; Hu, W.; Du, X. Collaborative Enhancement of Ce and Yb Addition to Microstructure and Mechanical Properties of In Situ Al6Si/5TiB2 Metal Matrix Composites. *J. Mater. Eng. Perform.* **2022**, 1–13. [CrossRef]
13. Raj, R.; Muchhala, D.; Kumar, R.; Gupta, G.; Sriram, S.; Chilla, V.; Mondal, D.P. Microstructure and Mechanical Properties of SiC/Mullite Reinforced A356 Composite Foam. *J. Mater. Eng. Perform.* **2022**, 1–16. [CrossRef]
14. Huang, Z.; Yan, H. Effect of Graphene on the Microstructure Evolution and Mechanical Properties of Al–10Si–2Cu–1.5Fe Aluminum Matrix Composites. *Int. J. Met.* **2023**, 1–10. [CrossRef]
15. Jia, X.Y.; Liu, S.Y.; Gao, F.P.; Zhang, Q.Y.; Li, W.Z. Magnesium matrix nanocomposites fabricated by ultrasonic assisted casting. *Int. J. Cast Met. Res.* **2009**, *22*, 196–199. [CrossRef]

16. Choi, S.M.; Awaji, H. Nano composites—A new material design concept. *Sci. Technol. Adv. Mater.* **2005**, *6*, 2–10. [CrossRef]
17. Sanaty-Zadeh, A. Comparison between current models for the strength of particulate-reinforced metal matrix nanocomposites with emphasis on consideration of Hall–Petch effect. *Mater. Sci. Eng. A* **2012**, *531*, 112–118. [CrossRef]
18. Bhushan, R.K.; Kumar, S.; Das, S. Fabrication and characterization of 7075 Al alloy reinforced with SiC particulates. *Int. J. Adv. Manuf. Technol.* **2013**, *65*, 611–624. [CrossRef]
19. Kumar, G.B.V.; Rao, C.S.P.; Selvaraj, N. Mechanical and dry sliding wear behavior of Al7075 alloy-reinforced with SiC particles. *J. Compos. Mater.* **2012**, *46*, 1201–1209. [CrossRef]
20. Kumar, A.; Pal, K.; Mula, S. Simultaneous improvement of mechanical strength, ductility and corrosion resistance of stir cast Al7075-2% SiC micro-and nano composites by friction stir processing. *J. Manuf. Process.* **2017**, *30*, 1–13. [CrossRef]
21. Modi, O.P.; Prasad, B.K.; Jha, A.K. Influence of alumina dispersoid and test parameter on erosive wear behavior of a cast zinc aluminium alloy. *Wear* **2006**, *260*, 895–902. [CrossRef]
22. Gencaga, P.; Temel, S. Dry sliding friction and wear properties of zinc-based alloys. *Wear* **2002**, *252*, 894–901.
23. Savaşkan, T.; Aydıner, A. Effects of silicon content on the mechanical and tribological properties of monotectoid-based zinc–aluminium–silicon alloys. *Wear* **2004**, *257*, 377–388. [CrossRef]
24. Ünlü, B.S. Investigation of tribological and mechanical properties of metal bearings. *Bull. Mater. Sci.* **2009**, *32*, 451–457. [CrossRef]
25. Khonsari, M.M.; Lin, Q. An investigation into the transient behaviour of journal bearing with surface texture based on fluid-structure interaction approach. *Tribol. Int.* **2018**, *118*, 246–255.
26. Ünlü, B.S.; Atik, E. Determination of friction coefficient in journal bearings. *Mater. Des.* **2007**, *28*, 973–977. [CrossRef]
27. Gupta, R.; Thakur, L. Development of an AA 7075 Wear-Resistant Coating on AA 6082 via Friction Surfacing: Optimization and Characterization. *J. Mater. Eng. Perform.* **2023**, 1–15. [CrossRef]
28. Eftekhar, A.H.; Sadrossadat, S.M.; Reihanian, M. Statistical Optimization of Electromagnetic Stirring Parameters for Semisolid AM60 Slurry Using Taguchi-Based Grey Relational Analysis. *Int. J. Met.* **2022**, *16*, 212–222. [CrossRef]
29. Şahin, Y. Preparation and some properties of SiC particle reinforced aluminium alloy composites. *Mater. Des.* **2003**, *24*, 671–679. [CrossRef]
30. Wu, L.; Yang, H.; Cheng, J.; Hu, C.; Wu, Z.; Feng, Y. Review in preparation and application of nickel-coated graphite composite powder. *J. Alloys Compd.* **2020**, *862*, 158014. [CrossRef]
31. Leng, J.; Wu, G.; Zhou, Q.; Dou, Z.; Huang, X. Mechanical properties of SiC/Gr/Al composites fabricated by squeeze casting technology. *Scr. Mater.* **2008**, *59*, 619–622. [CrossRef]
32. Guo, M.L.; Tsao, C.Y. Tribological behavior of aluminum/SiC/nickel-coated graphite hybrid composites. *Mater. Sci. Eng. A-Struct. Mater. Prop. Microstruct. Process.* **2002**, *333*, 134–145.
33. Dhoria, S.H.; Rao, V.D.P.; Subbaiah, K.V. Mechanical and wear behaviour of 6351 Al/Gr/SiC composites fabricated by squeeze casting. *Mater. Today Proc.* **2019**, *18*, 2107–2113. [CrossRef]
34. Madhukar, P.; Selvaraj, N.; Rao, C.; Kumar, G.V. Fabrication and characterization two step stir casting with ultrasonic assisted novel AA7150-hBN nanocomposites. *J. Alloys Compd.* **2020**, *815*, 152464. [CrossRef]
35. Mendoza-Duarte, J.M.; Robles-Hernandez, F.C.; Estrada-Guel, I.; Carreño-Gallardo, C.; Martínez-Sánchez, R. Aluminum Composites Reinforced with Graphite: A Densification and Mechanical Response Study. *MRS Adv.* **2017**, *2*, 2847–2855. [CrossRef]
36. Atla, S.; Kaujala, P.L. Investigation of graphite effect on the mechanical and tribological properties of Al 7075-SiC-graphite hybrid metal matrix composites. *Tribol.-Finn. J. Tribol.* **2020**, *37*, 26–32. [CrossRef]
37. Devaganesh, S.; Kumar, P.K.; Venkatesh, N.; Balaji, R. Study on the mechanical and tribological performances of hybrid SiC-Al7075 metal matrix composites. *J. Mater. Res. Technol.* **2020**, *9*, 3759–3766. [CrossRef]
38. Jayaprakash, D.; Niranjan, K.; Vinod, B. Studies on Mechanical and Microstructural Properties of Aluminium Hybrid Composites: Influence of SiC/Gr Particles by Double Stir-Casting Approach. *Silicon* **2022**, *15*, 1247–1261. [CrossRef]
39. Pawar, S.Y.; Kharde, Y.R. Effect of dual reinforced ceramic particles on elevated temperature tribological properties of hybrid aluminium matrix composites. *Adv. Mater. Process. Technol.* **2020**, *8*, 1104–1120. [CrossRef]
40. Rajaram, G.; Kumaran, S.; Rao, T.S.; Kamaraj, M. Studies on high temperature wear and its mechanism of Al–Si/graphite composite under dry sliding conditions. *Tribol. Int.* **2010**, *43*, 2152–2158. [CrossRef]
41. Babić, M.; Mitrovic, S.; Vencl, A. Tribological Characteristics of Aluminium Hybrid Composites Reinforced with Silicon Carbide and Graphite. A Review. *J. Balk. Tribol. Assoc.* **2013**, *19*, 83–96.